NCAR Auto-Nowcast System

C. MUELLER, T. SAXEN, R. ROBERTS, J. WILSON, T. BETANCOURT, S. DETTLING, N. OIEN, AND J. YEE

National Center for Atmospheric Research, Boulder, Colorado*

(Manuscript received 9 April 2002, in final form 27 January 2003)

ABSTRACT

The Auto-Nowcast System (ANC), a software system that produces time- and space-specific, routine (every 5 min) short-term (0–1 h) nowcasts of storm location, is presented. A primary component of ANC is its ability to identify and characterize boundary layer convergence lines. Boundary layer information is used along with storm and cloud characteristics to augment extrapolation with nowcasts of storm initiation, growth, and dissipation. A fuzzy logic routine is used to combine predictor fields that are based on observations (radar, satellite, sounding, mesonet, and profiler), a numerical boundary layer model and its adjoint, forecaster input, and feature detection algorithms. The ANC methodology is illustrated using nowcasts of storm initiation, growth, and dissipation. Statistical verification shows that ANC is able to routinely improve over extrapolation and persistence.

1. Introduction

This paper describes the Auto-Nowcast System (ANC), a software system that produces time- and space-specific 0–1-h nowcasts[1] of convective storm location and intensity. ANC combines meteorological observations, a numerical boundary layer model and its adjoint [Variational Doppler Radar Analysis System (VDRAS); Sun and Crook 2001], forecaster input, and feature detection algorithms to provide routine nowcasts of thunderstorm position. ANC was developed by the National Center for Atmospheric Research (NCAR) with prime funding from the Federal Aviation Administration (FAA).[2]

Early nowcasting techniques relied upon the simple extrapolation of storm positions. Even for periods less than 60 min, extrapolation nowcasts are often not useful because they fail to take into account storm initiation, growth, and dissipation. Wilson et al. (1998) provide a review of nowcasting systems and their capabilities. Existing extrapolation systems in the United States include (a) the Storm Cell Identification and Tracking (SCIT) algorithm used in the National Weather Service Warning Decision Support System (Johnson et al. 1998), and (b) the Thunderstorm Identification, Tracking, Analysis and Nowcasting algorithm (TITAN; Dixon and Wiener 1993) used in the National Convective Weather Forecast (Megenhardt et al. 2000) and elsewhere.

The need for more precise nowcasting has spawned four operational nowcasting systems that forecast storm initiation, growth, and dissipation. Two of these are used at the United Kingdom's Met Office: (a) GANDOLF (Generating Advanced Nowcasts for Deployment in Operational Land Surface Flood Forecast; Pierce and Hardaker 2000) and (b) Nimrod (Golding 1998). The third is the FAA Regional Convective Weather Forecast and Terminal Convective Weather Forecast system (Boldi et al. 2002). The fourth is ANC. Development of the latter two systems is jointly funded by the FAA AWRP. The ANC is currently operational at the Army Test and Evaluation Command meteorological units at White Sands Missile Range in New Mexico and Redstone Arsenal in Alabama. ANC was also deployed from 1997 to 2000 at the Washington–Baltimore National Weather Service Office in Sterling, Virginia, as part of the System for Convective Analysis and Nowcasting (SCAN) program (Smith et al. 1998). Efforts are under way to begin transfer of ANC components to the Advanced Weather Interactive Processing System (Smith et al. 1998). As part of the Sydney 2000 World Weather Research Program Field Demonstration Project (Keenan et al. 2003), Nimrod, GANDOLF, ANC, TITAN, and SCIT ran for a 3-

* The National Center for Atmospheric Research is sponsored by the National Science Foundation.

[1] The term nowcast is used in this paper to emphasize that the nowcasts are time and space specific for periods less than a few hours. The nowcasts may include initiation, growth, and dissipation of storms.

[2] FAA support is presently through the Aviation Weather Research Program (AWRP) as part of the Convective Weather Product Development Team (Wolfson et al. 1997). Additional support has been received from the Army Test and Evaluation Command (ATEC), National Science Foundation (NSF) portion of the U.S. Weather Research Program, and the Radar Operations Center of the National Weather Service.

Corresponding author address: Dr. Cynthia Mueller, NCAR, P.O. Box 3000, Boulder, CO 80307-3000.
E-mail: mueller@ucar.edu

month period at the Sydney office of the Australian Bureau of Meteorology.

A primary component of ANC is its ability to identify and characterize boundary layer convergence lines. Feature detection algorithms and VDRAS are used to monitor and nowcast boundary layer structure. The importance of the boundary layer in thunderstorm development was first shown by the Thunderstorm Project (Byers and Braham 1949). They found that boundary layer mesoscale convergence was a precursor to convective storm development. Purdom (1973, 1976, 1982) indicated the importance of monitoring cloud lines with satellite data to nowcast storms. Wilson and Carbone (1984) suggested the utility of radar-detected clear-air ''boundaries'' for use in thunderstorm nowcasting. Boundaries are defined here as narrow zones of boundary layer convergence associated with weather phenomena such as gust fronts, sea-breeze circulations, terrain-induced circulations, horizontal convective rolls, and synoptic-scale fronts. Forecasters worldwide appreciate the importance of boundaries in nowcasting convective storms. Wilson and Mueller (1993, hereafter WM93) provided conceptual models for using boundaries to nowcast thunderstorm evolution. These conceptual models form the basis for many of the nowcasting procedures utilized by ANC and are summarized in section 2. For a detailed discussion of the model, the reader is referred to WM93.

Section 2 describes and illustrates ANC methodology utilizing a case from the Washington–Baltimore area, section 3 summarizes a case study from the Denver area, section 4 summarizes performance statistics from White Sands and Sterling, and section 5 discusses ANC strengths, weaknesses, and potential improvements.

2. ANC system methodology

The practice of nowcasting requires the forecaster to review and assimilate a variety of disparate observations and model results within the context of their knowledge of how the atmosphere works (i.e., the ''conceptual model''). By the nature of the nowcast problem, the time available for the human to review data and make a nowcast is always very limited.

ANC mimics much of what is normally done by the human (but without feeling the time stress). It uses a data fusion system to assimilate a variety of datasets (which could include forecaster input) to create nowcasts that are issued at regular intervals (usually every 5 min) and that are based on conceptual models of how storm's initiate, grow, and dissipate. ANC uses a fuzzy logic system (e.g., McNeill and Freiberger 1993). Fuzzy logic provides an efficient manner to combine datasets and apply conceptual models. In meteorology, fuzzy logic has been used for a variety of applications including gust front detection and extrapolation (Delanoy and Troxel 1993), profiler winds analysis (Cornman et al. 1998), radar-based cloud particle typing (Vivekanandan et al. 1999), anomalous propagation (AP) detection and mitigation (Kessinger et al. 2001), icing detection (Bernstein et al. 2000), and turbulence detection and forecasting (Sharman et al. 2000). Fuzzy logic eliminates the binary yes–no decision required by decision trees and, instead, uses mathematical functions based on conceptual models to nowcast the likelihood of storms over a grid point in a defined region. Performance statistics are used to help tune the functions, but the fuzzy logic system is primarily physically based. Large datasets used by neural networks or other statistical techniques are not required to train or tune the system. Modifications to the fuzzy logic parameters can be made efficiently for different sites, weather conditions, and as new capabilities such as improved forecast models and more advanced observational systems become available.

ANC methodology is presented in this section by continued reference to a particular case study that shows a nowcast for the initiation of a squall line during the SCAN program. Figure 1a shows satellite data close to the time the nowcast was issued. The large line of clouds in Pennsylvania was associated with a cold front. The line of cumulus through northern Virginia and Maryland (within the white box) is the focus of this nowcast. Figure 1b shows for the same time the radar reflectivity and the low-level winds retrieved by VDRAS in a domain centered on the Sterling Weather Surveillance Radar-1988 Doppler (WSR-88D). A boundary is in evidence both from the VDRAS winds and from the line of enhanced reflectivity. This boundary was moving relatively slowly at 8 m s^{-1}. The steering level was from the west at $\sim$10 m s^{-1}. The line of cumulus quickly grew into a squall line that produced damaging winds and ¾- to 2-in.-diameter hail. ANC correctly nowcasts the initiation of the squall line. The Sterling National Weather Service Science and Operations Officer noted that ''Although our forecasters had discussed the potential for severe thunderstorms to break out, we were anticipating a late start based on extrapolation of the line of storms over Pennsylvania. The 2 June event underscores the critical nature of detecting boundaries to help in the convective initiation problem. . . . The automated forecast . . . actually showed potential for thunderstorms to form where they did prior to the thunderstorms actually forming'' (S. Zubrick 2000, personal communication). An example of a 30-min nowcast for initiation of echoes $\geq$35 dBZ and the nowcast verification is shown Fig. 2. This case will be used in the following section to illustrate the nowcast system's methodology.

a. Overview

Figure 3 provides a generalized schematic of the ANC system. The steps in producing the nowcast are briefly reviewed here to give an overview of the entire system. Operational datasets used in the system include full-

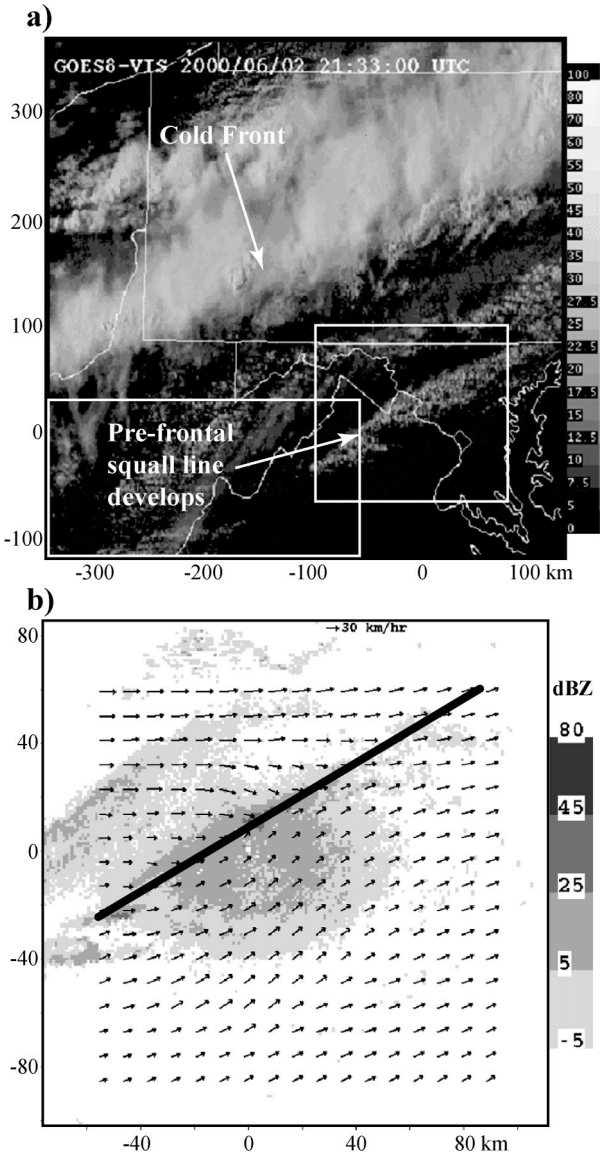

FIG. 1. (a) GOES satellite visible imagery at 2130 UTC 2 Jun 2000 over western PA, and northern WV, northern VA, and MD. Box indicates domain of (b). (b) Beam-to-beam radar reflectivity from the 0.5° elevation tilt, VDRAS low-level (180 m AGL) winds, and manually entered boundary location (solid line).

resolution radar (generally WSR-88D), satellite, surface stations (including special mesonets), lightning, profilers, numerical model, and radiosondes. These data are input into analysis algorithms to calculate predictor fields as shown in Fig. 3. Analysis algorithms include data quality control routines, feature detection algorithms, and VDRAS. In some cases, it is beneficial for a forecaster to interact with ANC by manually inputting the position of boundaries as shown in step 2. The forecaster-detected boundary positions are used as input into nowcast algorithms and to train the boundary detection algorithm. Because the boundary detection algorithm uses the forecaster input as guidance over a period of time, manually entering boundaries does not have to be done routinely.

The predictor fields are combined using a fuzzy logic approach as indicated in step 3. The fuzzy logic approach uses membership functions to map the predictor fields to the likelihood of storms (likelihood fields). The dimensionless likelihood fields are meant to represent the relationship between the predictor fields (listed in Table 2) and the existence of convective storms at validation time. These likelihood fields are not equivalent to probability; high values of likelihood for a single predictor field may have very low probabilities. The likelihood fields are weighted and summed to produce a combined likelihood field. The combined likelihood field is filtered and thresholded in step 4 to generate the nowcast areas of convective activity. In ANC deployments to date, the automated nowcasts are used as guidance by the forecasters.

b. Analysis algorithms, forecaster input, and resultant predictor fields (steps 1 and 2)

The first step in the ANC system is to process the observational datasets to produce predictor fields. Table 1 lists the analysis algorithms, input data streams, the purpose of each algorithm, and a numerical index to the derived predictor fields listed in Table 2. Table 2 lists the current ANC predictor fields along with a description of each field, its relative importance to the nowcast (relative weight used for the fuzzy logic summation), and references. These predictor fields are derived from conceptual models. The conceptual models are described in WM93 and are based on determining the overlap of regions where there is conditional instability (generally determined by cloud type and vertical development of the clouds), a favorable boundary to trigger convection, and the translated position and characteristics of current storms. Cloud fields are used to imply potential for convection initiation because no routine direct measurements of boundary layer thermodynamics (temperature and water vapor) are available on a temporal or spatial scale suitable for nowcasting. Convective storm initiation is very sensitive to the small-scale variations in boundary layer temperature and water vapor (Crook 1996) and the vertical depth of the boundary layer moisture (Mueller et al. 1993). Convective clouds provide an indication of where moisture may be sufficient for deep convection (Weckwerth 2000). Conversely, anvil-level cloud shields resulting from deep, moist convection can suppress new convection by stabilizing the air mass below the anvil.

WM93 provided a number of nowcast rules. Some examples of these rules include 1) if existing storms are moving in association with a boundary, the storms are nowcast to maintain and grow; 2) if there are clouds along two colliding boundaries, storms are nowcast to initiate and rapidly develop at the collision point, and

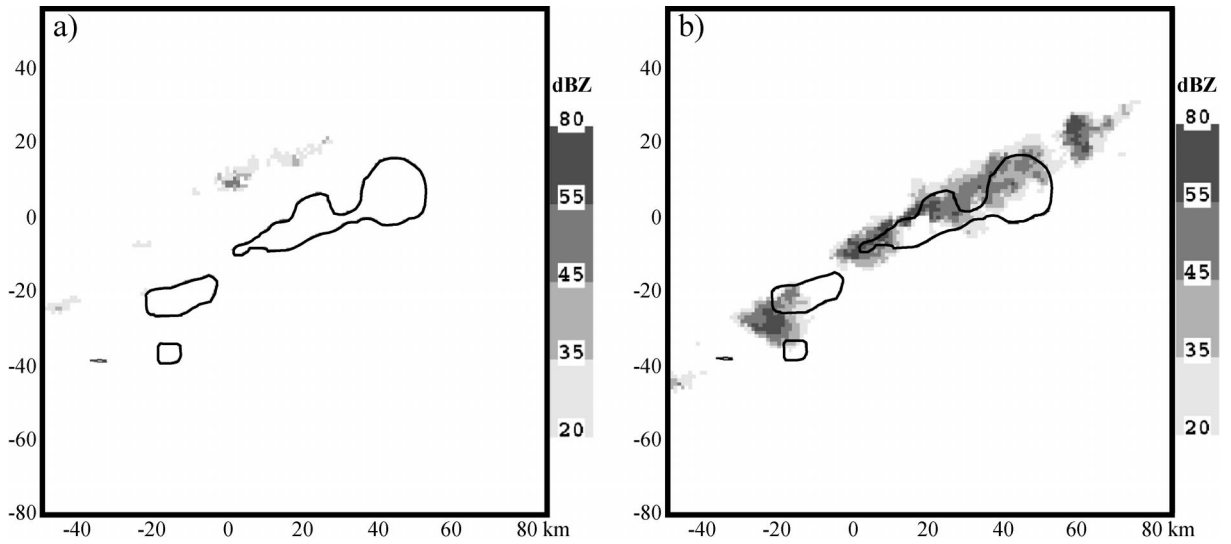

FIG. 2. Low-level (1.5 km MSL) radar reflectivity; the contour is the 30-min ANC nowcast. (a) The ANC 30-min nowcast at issue time, 2218 UTC 2 Jun 2000, and (b) the same nowcast superpositioned over reflectivity at verification time, 2248 UTC.

3) if a boundary moves rapidly away from a storm, the storm is nowcast to dissipate. In all these cases, information about the cloud field (used as a proxy for stability), boundary layer forcing (boundaries), and storm characteristics are evaluated and extrapolated in position to the 0–1-h nowcast time to determine the likelihood of storms at that time. The predictor fields in ANC reflect the rules described in WM93 and build on recent research (references listed in Table 2). In Table 2, the predictor fields are divided into information about storm characteristics (fields 1–5), boundary layer structure (fields 6–10), and cloud characteristics (fields 11–13).

1) STORM CHARACTERISTICS PREDICTORS

The storm characteristics predictors provide information to ANC about current storms. These predictor fields are based on storm area and trend information with time obtained by TITAN and on motion vectors obtained by the Tracking Radar Echo by Correlation (TREC) software package (Rineheart 1981; Tuttle and Foote 1990). Figure 4 shows the extrapolated gridded reflectivity field along with the ANC 30-min nowcast. Comparing the two nowcasts with the verification observations in Fig. 2b shows the extrapolation is useful, in that the motion of the line is captured. However, in this case there was considerable growth of the storm that was not captured by extrapolation alone. Although storm history is useful to the ANC system, storm characteristics and trends by themselves do not provide sufficient information to nowcast storms because the physical processes that influence how a storm will change in the future are not fully reflected in the storm's past (Tsonis and Austin 1981; MacKeen et al. 1999). One of the primary nowcast predictor fields is the extrapolated reflectivity based on the TREC software package.

Motion vectors for the extrapolation nowcasts are based on filtered radar-reflectivity data. An ''elliptical'' filter (Wolfson et al. 1998) is used to smooth and remove the small and more perishable scales from the reflectivity field. Typical dimensions of the filter are 5 km by 19 km. The elongated shape of the elliptical filter enhances the linear features allowing TREC to capture the propagation speed of the line or area as opposed to individual cell motions. A 1-km gridded reflectivity field is extrapolated using the TREC motion vectors and the resultant field is the extrapolation nowcast field.

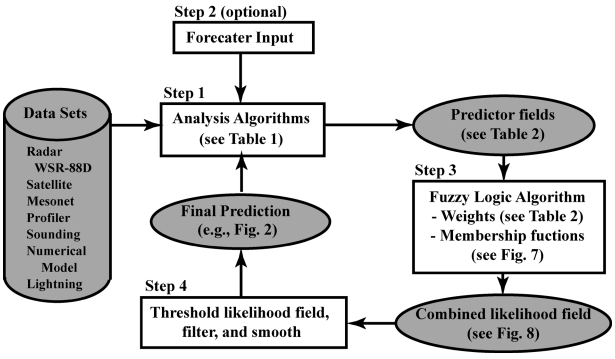

FIG. 3. Schematic of ANC. Boxes indicate algorithmic steps (software processes and human input). Shaded areas indicate data and various predictor and nowcast fields.

2) BOUNDARY LAYER CHARACTERISTICS PREDICTORS

The detection of boundary layer convergence lines is crucial to nowcasts of initiation, growth, and dissipation of storms. ANC uses boundary layer predictor fields to

TABLE 1. List of system processes (analysis algorithms) used in ANC, including the data software processes they employ, the purpose of the algorithm, and the fields predicted (the numbers refer to the list of predictors in Table 2). VAD refers to Velocity Azimuth Display; RUC refers to the Rapid Update Cycle.

Software name	Data	Purpose	Predictor fields
Elliptical filter	Cartesian radar	Filter perishable scales	1, 2
TREC	Same as above	Extrapolate radar reflectivity	1, 2, 3, 4
TITAN	Same as above	Storm characteristics and trends	3, 4
Precip accumulation	Same as above	Calculate precipitation accumulation based on standard Z–R relationship	5
COLIDE	Human-inserted boundaries	Extrapolates boundary position	6, 7, 8, 9, 10
VDRAS	High-resolution radar data, mesonet data and VADs from surrounding radars	Cloud-scale numerical model and its adjoint used for single radar retrieval of boundary layer winds and thermodynamics	9, 10
Boundary collision and boundary-storm collision	COLIDE extrapolations, TITAN, and steering flow from profiler or RUC data	Delineates regions where a boundary collision, boundary intersection, or boundary–storm collision will take place	7
Boundary grid	COLIDE extrapolations, steering flow, and VDRAS winds	Delineates regions associated with boundary lifting and provides boundary layer characteristics in those regions	6, 8, 9, 10
Satellite applications	GOES satellite visible and IR data	Provides information about cloud type and growth	12, 13, 14

quantify the characteristics of boundaries and relate this to their likelihood to trigger storms. Boundary location and motion are obtained by use of automated feature detection algorithms such as the Machine Intelligent Gust Front Algorithm (MIGFA; Delanoy and Troxel 1993) or Convergence Line Detection (COLIDE; Roberts et al. 1999). MIGFA and COLIDE detect, track, and extrapolate the positions of boundaries. The COLIDE algorithm can be run in automated or interactive modes. Boundary detection has proven to be a difficult topic. Although the human eye can often detect features in radar, satellite, and mesonet data that indicate the presence of a boundary, it is difficult to build an algorithm that consistently detects the boundaries' more subtle features without inducing false detections. The forecaster can manually enter boundaries that guide the automated algorithms (step III in Fig. 3). Thus the forecaster enhances the nowcast without interfering with routine ANC output. COLIDE runs continually with or without human input. If the forecaster enters a boundary manually, then COLIDE uses the forecaster's input to enhance the boundary detections. The future position of the boundary is based on extrapolation of recent positions.

Once boundary location and motion are established, ANC calculates gridded predictor fields. The boundary predictor fields are obtained from the 1) boundary motion, 2) steering-level winds (obtained from sounding or numerical model data), and 3) VDRAS. VDRAS retrieves a 3D wind and thermodynamic analysis of the boundary layer based on single-Doppler radar and mesonet data. An example of one of the boundary layer predictor fields is shown in Fig. 5. Figure 5a shows the VDRAS vertical velocity (w) data and boundary position information used to create the so-called MaxW predictor field (see Fig. 5b). The MaxW predictor field is calculated in a three-step process. First, the w values are assigned to discrete 10-km boundary segments using the maximum value of the VDRAS vertical velocity at ~1 km above ground level (AGL) along the segment. Second, the boundary position is extrapolated. Finally, the grid around the extrapolated boundary position is populated with the MaxW values assigned to the boundary segments. The resulting field (Fig. 5b) shows an elongated feature that surrounds the position of the extrapolated boundary. The cross-boundary width of the elongated MaxW field is based on statistical studies of storm initiation and growth relative to boundaries (Wilson and Schreiber 1986; Mueller et al. 1997). In the case of moving boundaries, one-third of the field is placed in front of the boundary and the cross-boundary width is generally 25 km. The region around stationary boundaries is centered on the boundary and the width is 15 km. Other boundary layer predictors are summarized in Table 2.

3) CLOUD CHARACTERISTICS PREDICTORS

ANC uses cloud characterization fields as indicators of instability. The cloud predictor fields are based on either satellite or radar data. The Geostationary Operational Environmental Satellite (GOES) data are used to indicate regions of cumulus and cumulus congestus based on cloud-type algorithms (Bankert 1994; Roberts 1997). In addition to cloud type, the change in GOES IR temperature (channel 4, 11 μm) is monitored as an indicator of vertical cloud growth (Roberts 1997; Roberts and Rutledge 2003).

TABLE 2. List of predictors used in ANC. A brief description of the field is provided along with the relative weights used in the fuzzy logic algorithm (the relative importance of each of the fields), and references. The weights shown here are not meant to add to 1.0.

Predictors (units)	Description	Weight	Reference
1) Extrapolated reflectivity (dBZ)	Indicates extrapolated position of radar echoes	0.20	Ligda (1953); Wolfson et al. (1998)
2) Extrapolated reflectivity with stratiform regions removed (dBZ)	Highlights convective regions	0.40	Steiner et al. (1985)
3) Storm area (km^2)	Provides area enclosed by 35-dBZ contour; area is used as an indicator of storm lifetime	0.20	Wilson (1966)
4) Negative and positive growth rates ($km^2\ h^{-1}$)	Indicates growth rate of storm area; used alone, storm trending does not provide good nowcasts—however, when used in combination with environmental information, storm trends are valuable	0.15	Tsonis and Austin (1981)
5) Precipitation accumulation (mm)	Derives 1-h precipitation accumulation based on standard *Z–R* relationship; the field is used to suppress nowcast for convection in areas where it has rained	0.15	Wilson and Mueller (1993)
6) Boundary location and speed ($m\ s^{-1}$)	Indicates location where convection is likely to be triggered by boundary layer convergence line	0.20	Wilson and Schreiber (1986)
7) Boundary collision and storm–boundary collision	Location of a boundary collision tends to be more favorable for storm development because of enhanced vertical velocities and favorable low-level shear	0.25	Rotunno et al. (1988)
8) Boundary-relative steering flow ($m\ s^{-1}$)	Measure of how clouds are moving relative to the boundary; if the boundary relative steering flow is small ($<6\ m\ s^{-1}$), clouds that form along the boundary and move with the steering flow will stay in proximity of the boundary and presumably a sustained updraft; these clouds are more likely to develop into thunderstorms than clouds in regions where there is a large boundary-relative steering flow ($>10\ m\ s^{-1}$)	0.20	Wilson and Mueller (1993)
9) Boundary-relative low-level shear ($m\ s^{-1}$)	Measure of the potential for deep updrafts; in situations where there is strong low-level shear ($<12\ m\ s^{-1}$), the horizontal vorticity associated with the density current or boundary is more likely to match the environmental horizontal vorticity; when the horizontal vorticity between the density current and environment are roughly equal in magnitude and opposite in direction, the corresponding updraft is vertical and more favorable for thunderstorm development	0.20	Wilson and Megenhardt (1997)
10) MaxW ($m\ s^{-1}$)	Measure of the vertical velocity associated with the boundary	0.20	
11) Radar Cu (dBZ)	Indicates regions of growth aloft based on radar reflectivity; a three-step process is used to calculated this predictor field; first the maximum reflectivity in a column that extends between 3 and 6 km AGL is obtained; the field is filtered using the stratiform–convective partitioner to remove stratiform echo; finally the field is advected with steering flow winds	0.25	Wilson and Mueller (1993); Henry and Wilson (1993)
12) Satellite cloud type	Indicates cloud types based on satellite albedo and IR data; cumulus clouds are used to imply atmospheric stability; regions where cumulus clouds are present in association with horizontal convective rolls or boundaries are more favorable for storm development	0.15	Mueller et al. (1993); Roberts (1997); Weckwerth (2000)
13) IR temp cooling (°C per 15 min)	Measure of change in IR temperature over 15 min; cooling cloud-top temperatures in regions where cumulus clouds are present along with boundary layer convergence provides indication of cloud growth	0.25	
13) IR temp–clear	Delineates clear-sky regions based on IR data; used to suppress nowcasts for thunderstorms	0.15	
14) Terrain	Used at WSMR to increase the likelihood of convection over mountains and to decrease the likelihood in the basin region	0.15	Saxen et al. (1999)

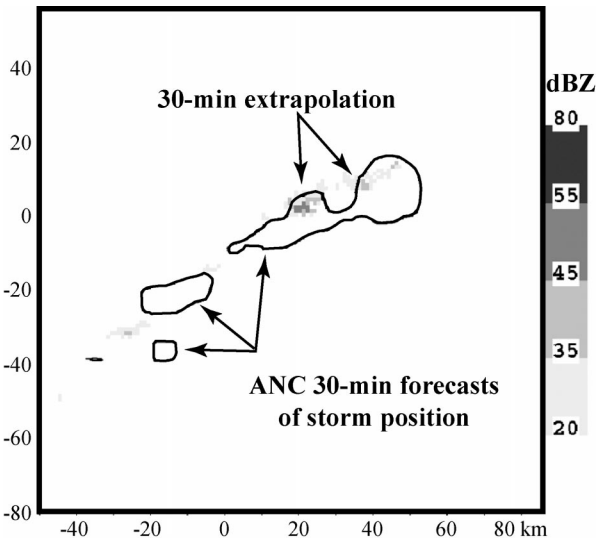

FIG. 4. Comparison of 30-min ANC output and echo extrapolation (gray shades) nowcasts. Verification of these nowcasts is shown in Fig. 2b.

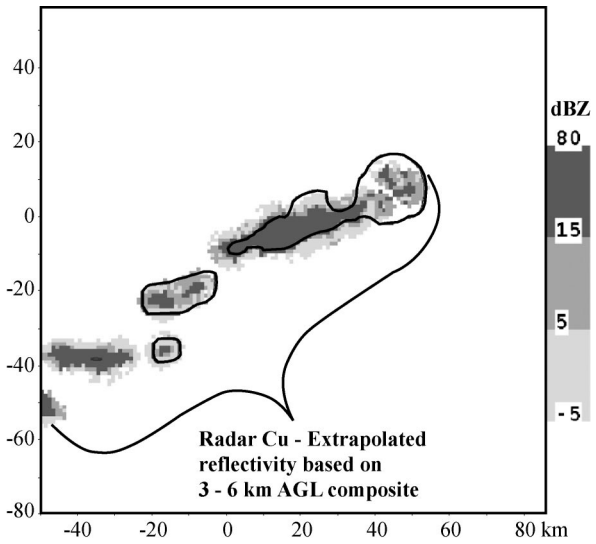

FIG. 6. The Radar Cu predictor field is shown along with ANC 30-min nowcast (black lines).

When satellite data are not available or the low-level clouds are obscured by upper-level cloudiness, radar data are used. Knight and Miller (1993) showed that sensitive radars similar to the WSR-88Ds are capable of detecting early cumulus clouds prior to the development of precipitation size particles. Strong gradients in moisture along the cloud edges produce weak echoes (<5 dBZ) from Bragg scattering that are called mantel echoes. However, the WSR-88D scan strategy is not optimal for detecting these shallow clouds (Roberts 1997). In addition, algorithms cannot easily discern weak echo associated with developing cumulus from weak echo associated with other weather such as stratiform debris. Therefore, the earliest stage of cumulus development that ANC detects routinely is cumulus congestus.

Figure 6 illustrates the Radar Cu predictor field (Table 2) showing the presence of convective echoes between 0 and 55 dBZ in the height range of 3–6 km. ANC allows cloud fields determined by radar and satellite to be extrapolated in many ways based on user input. Generally the steering-level winds obtained from soundings, profilers, or numerical model data are used. However, calculating a good motion vector for the cloud fields is a major challenge. Sometimes the observed clouds remain fixed to the boundary and other times move with the mean flow in the volume of the space they occupy.

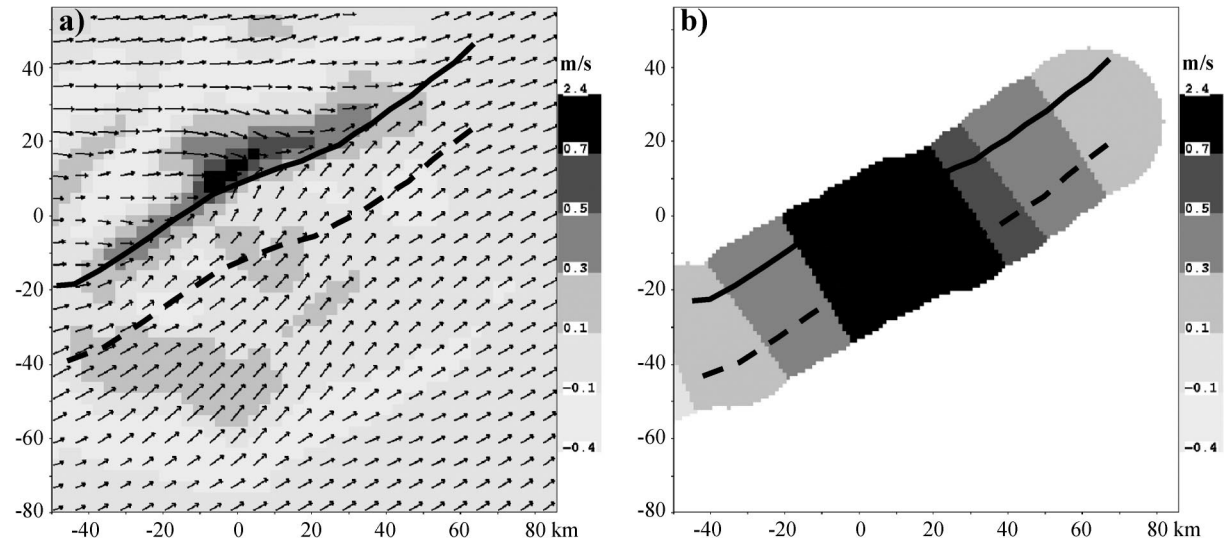

FIG. 5. (a) VDRAS horizontal wind vectors (180 m AGL) and vertical velocity field (gray shades) at 940 m AGL, and (b) MaxW predictor field in gray shades. The boundary position is shown as a solid line and 30-min extrapolation as a dashed line.

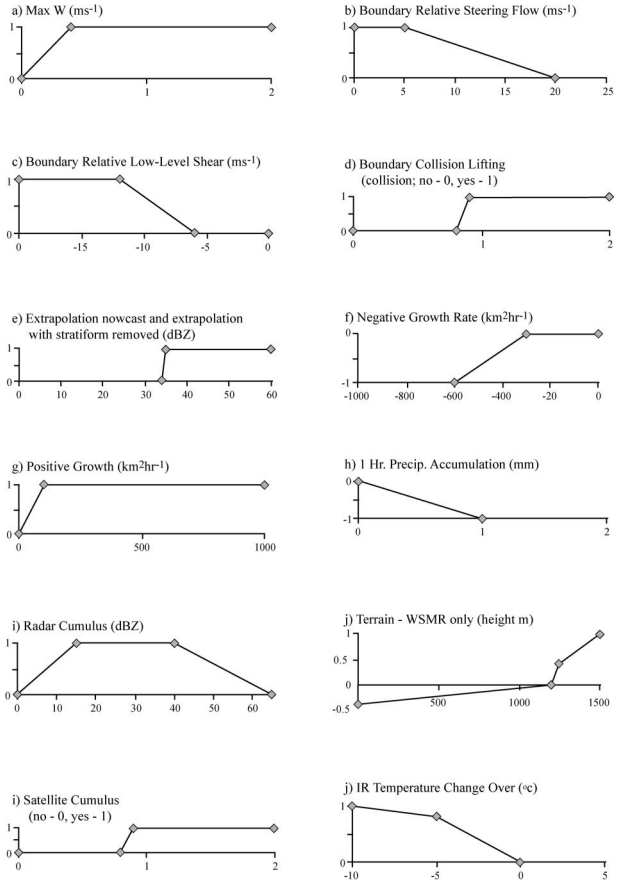

FIG. 7. (a)–(j) Common membership functions used in ANC.

TABLE 3. Verification statistics for the ANC nowcast shown in Fig. 2, extrapolation shown in Fig. 4, and persistence. A reflectivity of 35 dBZ is used to define extrapolation and persistence forecasts and as the threshold for the observations.

	POD (%)	FAR (%)	CSI (%)	Bias
ANC	38.3	54.8	26.1	0.85
Extrapolation	3.8	0	3.8	0.04
Persistence	0	100	0	0.04

The Radar Cu field shown in Fig. 6, for example, is extrapolated by using the boundary motion.

c. Fuzzy logic algorithm and nowcast (steps 3 and 4)

Nowcasts are obtained by converting the predictors just discussed (and summarized in Table 2) to likelihood fields using the membership functions shown in Fig. 7, weighting the importance of each field to the nowcast, and summing. The membership functions are based on one's insight into the physical processes taking place, and converting the predictors into the dimensionless likelihood fields. These likelihood fields have a dynamic range from -1 to 1; increasing positive numbers are used to indicate a region of increasing likelihood of storms, decreasing negative numbers indicate regions of decreasing likelihood, and zero indicates neutral likelihood. The various likelihood fields are weighted using the values shown in Table 2 and the results are summed to produce the combined likelihood field. The combined field is filtered, smoothed, and then thresholded to provide the final nowcast.

Figure 8a shows the combined likelihood field for the example case. In this relatively simple case, the contributions of various predictors are identified. The elongated-shaped region is associated with boundary char-

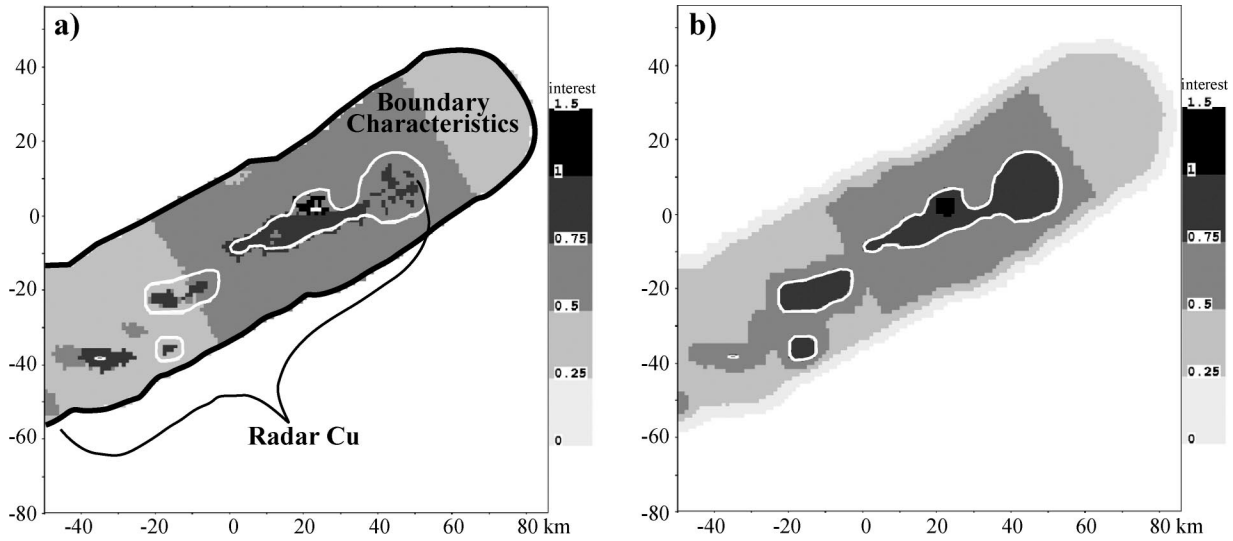

FIG. 8. (a) Combined-likelihood field for the relatively simple nowcast shown in Fig. 2. (b) Filtered combined likelihood field that is thresholded (white contour) to produce the final nowcast.

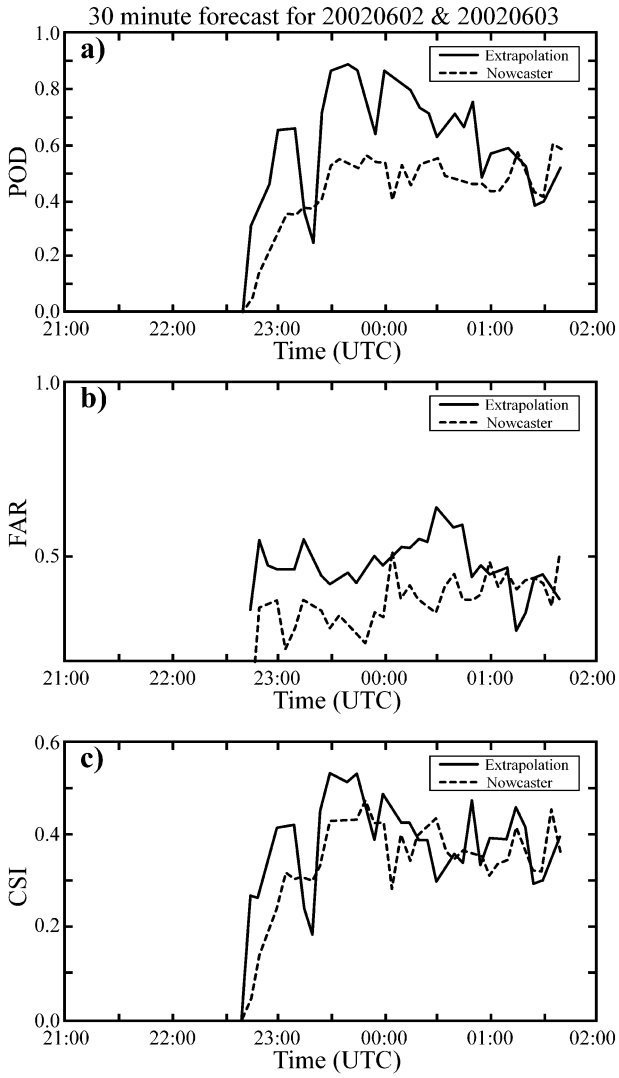

FIG. 9. Nowcast statistics for 2 Jun 2000. The 30-min nowcasts issued at 5-min intervals are evaluated. Times are verification time. Extrapolation nowcasts are shown in solid line, ANC nowcasts in dashed line.

acteristics. The Radar Cu and extrapolated reflectivity positions lead to enhanced values of the combined likelihood field and hence increased likelihood of storms. [Satellite predictors were not used in this example. Roberts and Rutledge (2003) show nowcasts from this case with and without satellite predictor fields.] In effect, the combined likelihood field provides a method of determining the overlap of the various predictors and hence the expected regions of storms.

The combined likelihood field is filtered and thresholded to produce the final forecast (see Fig. 8b). The filter type varies depending on the locations of the boundaries. In the area outside of the elongated feature that surrounds the position of the extrapolated boundary, small nowcast regions of high combined likelihood are removed and large regions are generally reduced (whether the region is reduced and the extenet of the reduction is dependent on the magnitude of the combined likelihood field). Inside the elongated features, the nowcast regions are enlarged. The resultant field, Fig. 8b, is thresholded to provide the nowcast. The value used to threshold the field is determined by data review and statistical evaluation.

d. Verification

This section provides a review of the verification methodology, and section 4 discusses verification statistics in detail. Contingency tables based on grid-to-grid comparison of the nowcast and observed fields (Doswell 1986) are used to calculate the probability of detection (POD), false-alarm rate (FAR), and critical success index (CSI). A perfect score for POD is 100%, FAR is 0%, and CSI is 100%. Persistence, extrapolation, and ANC statistics are generally evaluated and compared. Generally the verification field (observation) is a constant-altitude plot of radar reflectivity measurements at a height of 1.5 km AGL. A 35-dBZ threshold is used to delineate the storm–no-storm boundary.

The POD, FAR, and CSI values for the extrapolation and ANC nowcasts shown in Fig. 4 (observations are shown in Fig. 2b) are given in Table 3. Although the nowcast is quite accurate, the value of the nowcast statistics are relatively low. In fact, the 1-km grid-to-grid comparison is a very stringent verification approach and the actual magnitudes of the statistics are not intuitively meaningful. In addition, the magnitudes of the statistics are strongly dependent on the methodology used in the calculations. Therefore, in order to glean useful information from the statistics, comparisons with other baseline nowcast techniques such as persistence and extrapolation are necessary. In this case, persistence has no skill (Table 3). ANC improves over extrapolation in terms of POD and CSI. The FAR is much higher for the ANC system because the extrapolated reflectivity echo was very small in comparison to the ANC forecast.

Time series statistics for the 2 June 2000 ANC and extrapolation nowcasts are shown in Fig. 9. ANC consistently provides superior results as compared to extrapolation for both POD and CSI. This improvement is shown for all time periods but is especially evident in the initial nowcast periods. The importance of including accurate boundary motions into the analysis is shown by the dip in ANC POD and FAR scores at ~2318 UTC. The boundary motion was incorrectly nowcast to increase but instead the motion remained steady. The resultant ANC nowcast mislocated the boundary and the Radar Cu field (that was advected with the boundary motion) based on faster than actual motion, resulting in the poor scores.

3. Examples of initiation, growth, and dissipation nowcasts

This section presents examples of initiation, growth, and dissipation nowcasts using a case on 5 July 2001

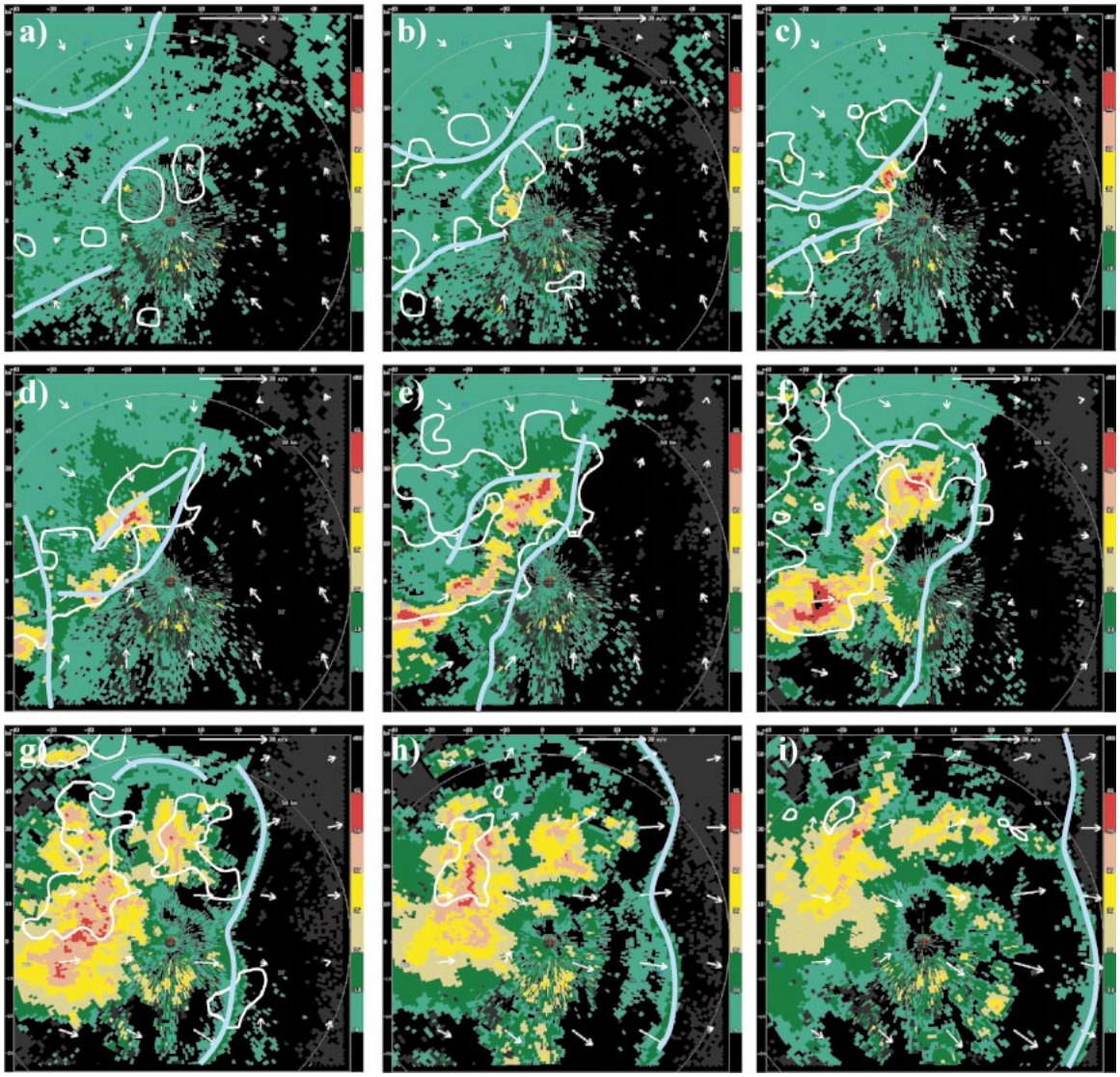

FIG. 10. ANC 30-min nowcasts for Denver, CO, area. The frames are at 18-min intervals from (a) 2354 UTC 5 Jul to (i) 0218 UTC 6 Jul 2001. White vectors indicate VDRAS low-level winds and the cyan lines are human-generated boundaries. The white contours are 30-min nowcasts issued at the time of radar PPIs shown. The radar echoes that existed at the corresponding verification times are shown in Fig. 11. Light green represents 0–10 dBZ; dark green, 10–25 dBZ; khaki, 25–35 dBZ; yellow, 35–45 dBZ; pink, 45–55 dBZ; and red, >55 dBZ.

in the Denver, Colorado, area. On this day, synoptic-scale forcing over Colorado was weak. The steering-level winds were approximately 5 m s^{-1} from the southeast. Surface dewpoints were ~10°C, which are typical values observed on days when thunderstorms occur in the Denver area in the summer convective season. Storms formed, grew, and dissipated within the ANC domain. During the storms, Denver International Airport's ground operations were shut down for over an hour while the storm produced a good deal of lightning and hail.

The 30-min ANC nowcasts are shown in Fig. 10 by the white lines with the corresponding verification data shown in Fig. 11. The nine panels are at 18-min intervals. The nowcasts shown in Figs. 10a and 10b predict the initiation of storms associated with a boundary collision. In Figs. 10c,d,e storms have already initiated and the nowcasts are for storm growth. Last, in Figs. 10f,g,h,i, the nowcasts predict storm dissipation as the boundary moves away from the storm. In general, ANC nowcasts for both 30 and 60 min are quite good.

A time series of area coverage of 35 dBZ or greater observations, Fig. 12, illustrates the rapid development and dissipation of the system. The time periods of initiation (I), growth (G), and dissipation (D) are labeled on the graph. The nowcast statistics for the 30- and 60-min nowcasts are shown in Fig. 13. Four nowcast techniques were evaluated: 1) persistence, 2) extrapolation,

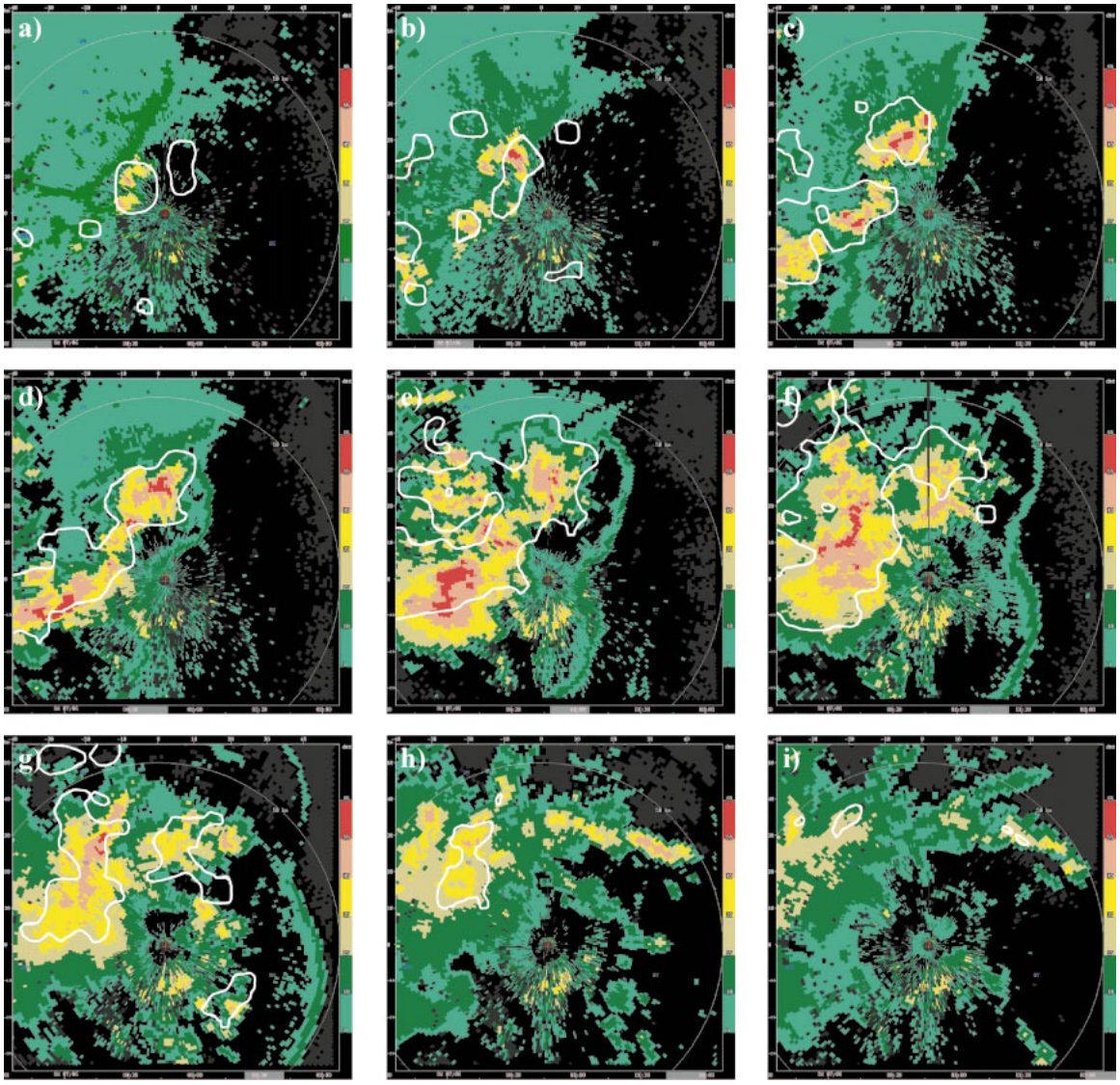

FIG. 11. The verification images for the nowcast shown in Fig. 10.

3) ANC with automated boundaries, and 4) ANC with human-generated boundaries. Statistics are based on a 1-km grid-to-grid comparison. Times of initiation, growth, and decay are indicated. Table 4 lists the relative contributions of ANC predictor fields for 30- and 60-min initiation, growth, and dissipation portions of the nowcasts. The table shows a subjective evaluation of which predictors were the most important to the nowcasts. The satellite fields were not useful on this day because high-level cirrus from mountain convection obscured low-level clouds.

Figures 13a,c,e show that the 30-min ANC skill scores using automated and human boundary inputs are almost equivalent during the initiation and growth stages. Review of the nowcasts shows that ANC with human-generated boundaries covered slightly larger areas than the automated version, but the nowcast locations were basically the same. However, the automated and human-generated boundaries used by ANC were not the same. The automated system only captured the boundary coming from the north and the motion vector was too fast. Even with the poor detection by the automated system, both human and automated systems had boundary-relative steering-level speed fields that were favorable for initiation and that overlapped with a Radar Cu field. Thus, both automated and human systems met the minimum requirements for an initiation nowcast and because the Radar Cu field was the same for both systems, the nowcasts were similar. In the case of the 60-min nowcasts, the verification statistics (Figs. 13b,d,f) indicated that the human-generated boundary nowcasts captured the initiation 30 min prior to the automated system. At 60 min the boundary characteristics were the primary contributors to the nowcasts and, in this case,

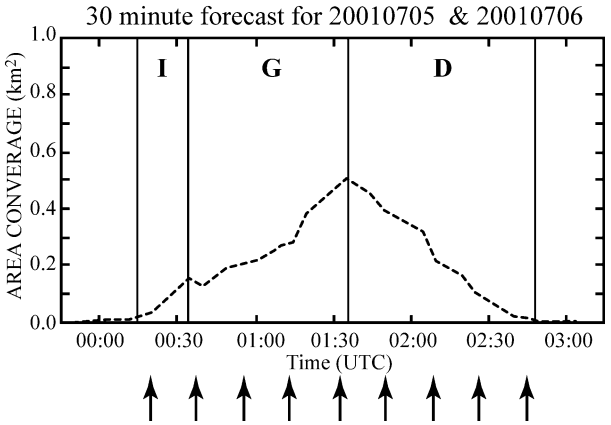

FIG. 12. Area coverage of time series for the 5–6 Jul case. Verification times for nowcasts shown in Figs. 10 and 11 are indicated by arrows. Initiation (I), growth (G), and dissipation (D) phases are indicated.

boundary collision was the most important field. The automated system was unable to detect either of the southern boundaries and therefore missed the collision and did not produce a timely initiation nowcast.

The nowcasts for continued growth at both 30 and 60 min were based heavily on a strong positive vertical motion determined from VDRAS winds, storm–boundary collision, and positive storm area growth. The 30-min nowcast also uses Radar Cu. For the 30-min nowcast, the extrapolated storm positions, Radar Cu, and storm area trend play a much larger role than in the 60-min nowcast. The 60-min nowcast is more dependent on the environmental conditions associated with the boundaries (e.g., MaxW) and storm–boundary collision.

Finally, during the dissipation stage, both the 30- and 60-min nowcasts were based on the absence of a boundary and negative growth rates.

Short-term nowcasts of less than 30 min depend primarily on accurate detection and extrapolation of the cumulus field either as determined by satellite or radar, or by storm trends in association with a boundary. As the nowcast period increases, accurate knowledge of the boundary layer structure and stability become more important. In all cases, accurate extrapolations of the various fields are required and are often difficult to obtain thus decreasing the potential spatial accuracy of the nowcast.

4. Performance statistics

ANC has been run in several different environments. The Sterling, Virginia, region that is used in this study is characterized by relatively strong synoptic-scale forcing and thunderstorms, which form into large, long-lived multicellular lines. Steering-level winds are generally brisk (>12 m s^{-1}), and the multicell lines are driven primarily by advection from the steering-layer flow. A good radar echo extrapolation is a required element of a good nowcast. Widespread thunderstorm initiation is relatively rare. However, thunderstorm complexes do evolve rapidly and require the extrapolation nowcasts to be augmented with nowcasts of thunderstorm growth and decay.

In contrast, the White Sands, New Mexico, region tends to have very weak synoptic-scale forcing. Thunderstorm activity is generally isolated and short lived. Steering-level winds are generally weak, <5 m s^{-1}, and storms tend to be slow moving or stationary; a persistence nowcast often shows more skill than an extrapolation nowcast especially over the mountainous terrain. Because the storms are short lived, nowcasts of storm initiation and dissipation are crucial to the nowcast problem. The Denver, Colorado, region represents a mix between these two extremes. In spring and early summer, synoptic-scale forcing is frequently a factor in convective development. During the remainder of the convective season synoptic forcing is weak, and boundaries produced by a variety of mechanisms are common and they tend to control storm evolution.

Because of the different weather conditions, terrain, and available observations, each of the ANC sites just mentioned used a different set of predictors. For instance, VDRAS was not run at White Sands due to the mountain–valley terrain; therefore, the boundary-relative low-level shear and MaxW were not available. At Sterling and Denver, high-level clouds often obscured the underlying cumulus so that the satellite fields provided little information. However, in White Sands, the satellite data were almost always useful for initiation and growth nowcasts. The time periods also varied among the sites. For the short-lived storms at White Sands, nowcast periods longer than 30 min showed little skill. At Sterling and Denver accurate nowcasts out to an hour were achieved.

The summary statistics presented in this paper provide some limited operational evaluation of the utility of ANC. Examples of verification statistics are shown for Sterling and White Sands operational nowcasts. Figure 14 shows 30-min nowcast statistics calculated for eight Sterling and five White Sands case study days representing 22 and 24 h of data, respectively. The days were chosen based on the occurrence of convective activity and the existence of complete datasets. Boundary positions were entered by a human. The POD and CSI scores in Fig. 14 indicate that in all Sterling cases, ANC shows improvement over extrapolation. ANC skill scores (Wilks 1995) are calculated using

$$\mathrm{SS}_{\mathrm{ref}} = \frac{A - A_{\mathrm{ref}}}{A_{\mathrm{perf}} - A_{\mathrm{ref}}} \times 100\%.$$

where A is a measure of accuracy, A_{ref} is a set of reference forecasts, and A_{perf} is the value of the accuracy measure that would be achieved by perfect forecasts. The numerical values shown in Fig. 14c are calculated using CSI for the measure of accuracy, A. The reference

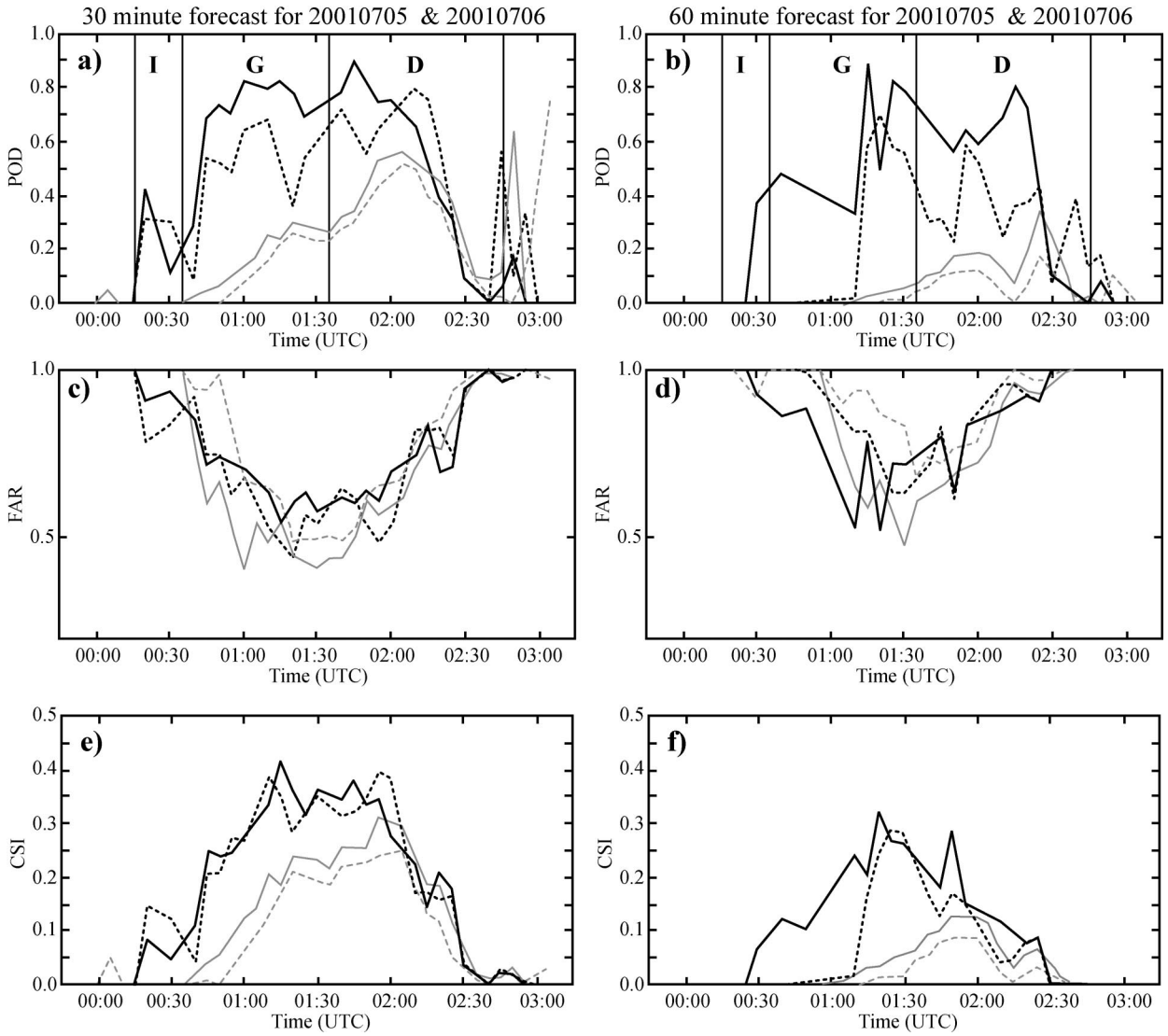

FIG. 13. Verification statistics for 30- and 60-min nowcasts for 5–6 Jul 2001 (verification times) are shown. POD scores for (a) 30- and (b) 60-min nowcasts, FAR for (c) 30- and (d) 60-min nowcasts and (e), (f) CSI. The broken light gray, solid light gray, broken black, and solid black lines show nowcasts for persistence, extrapolation, ANC with automated boundaries, and ANC with forecaster-generated boundaries. Initiation (I), growth (G), and dissipation (D) phases are indicated.

forecast is extrapolation and the A_{perf} is set to one. Scores range from 12% for a White Sands case where there was a significant amount of growth and decay to 2% for a Sterling case that was primarily advection of a squall line. For Sterling, in six of the eight days, ANC has slightly lower FAR than extrapolation. Conversely, ANC FARs for White Sands tended to be slightly higher than extrapolation. This is the result of overnowcasting thunderstorm initiation.

White Sands real-time verification statistics for 30-min nowcasts are shown in Figs. 15 and 16. These statistics are based on a fully automated system and encompass daytime nowcasts (from 0800 to 2000 LT) during July and August 2000. Satellite data are used routinely (Roberts and Rutledge 2003). In general, Fig. 15 shows that the ANC POD is better than the PODs for extrapolation and persistence. However, the FAR tends to be slightly higher for ANC and thus the CSI scores are similar for extrapolation and ANC nowcasts. Distributions of the differences in ANC and extrapolation nowcast CSI scores are shown in Fig. 16. The distribution shows that about a third of the time the difference is near zero. However, in a majority of the cases the nowcasts show improvement over extrapolation and the distribution is strongly skewed to the right. Review of these nowcasts shows that the majority are associated with forecasts of initiation or growth. The relatively frequent successes of ANC tend to be diluted in the review of only summary statistics, particularly during periods dominated by strongly forced synoptic convec-

TABLE 4. List of predictors used in ANC, Table 2, along with their subjective contribution to the 5 Jul 2001 forecast of initiation, growth, and dissipation. A 1 indicates it was a major factor, 2 indicates a significant factor, and 3 a contributing factor.

Predictors (units)	Initiation		Growth		Dissipation	
	30 min	60 min	30 min	60 min	30 min	60 min
1) Extrapolated reflectivity (dBZ)			1	2		
2) Extrapolated reflectivity with stratiform regions removed (dBZ)			3	3		
3) Storm area (km^2)			3	3		
4) Negative and positive growth rates (km^2 h^{-1})			1	2	1	1
5) Precipitation accumulation (mm)						
6) Boundary location and speed (m s^{-1})	3	3	3	3	1	1
7) Boundary collision and storm–boundary collision	2	1	1	1		
8) Boundary-relative steering flow (m s^{-1})	1	2	2	2		
9) Boundary-relative low-level shear (m s^{-1})						
10) MaxW (m s^{-1})	1	1	1	1		
11) Radar Cu (dBZ)	1		2			
12) Satellite cloud type						
13) IR temp cooling (°C over 15 min)						
14) IR temp–clear						

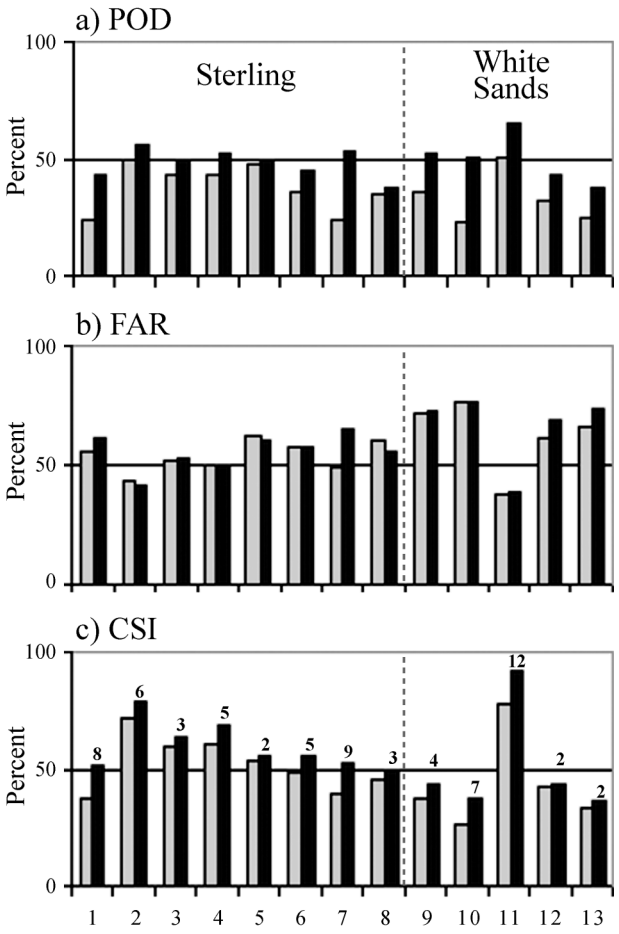

FIG. 14. Summary statistics from Sterling, VA, and White Sands, NM, case study days. The light gray bars to the left and black bars to the right represent the extrapolation and ANC nowcasts scores, respectively. (c) Numerical ANC skill scores in relation to extrapolation and based on CSI for each day.

tion where large areas of echoes are rapidly advected. A successful nowcast of the initiation of a line of storms as demonstrated earlier for 2 June is of major operational significance. However this significance is poorly reflected due to limitations in the statistics presented here.

5. Conclusions

ANC is used to its best advantage in the prediction of boundary layer–forced storms, and it performs well in conditions of both weak (White Sands) and strong (Sterling) synoptic forcing. Boundary detection and characterization are crucial to nowcasts of storm initiation, growth, and dissipation. Automated boundary detection algorithms tend to provide adequate skill for a 30-min storm forecast because the nowcasts are pri-

	POD	FAR	CSI	Bias
Persistence	27.7%	69.7%	16.9%	0.91
Extrapolation	31.7%	63.5%	20.4%	0.87
Nowcast	41.4%	69.8%	21.2%	1.37

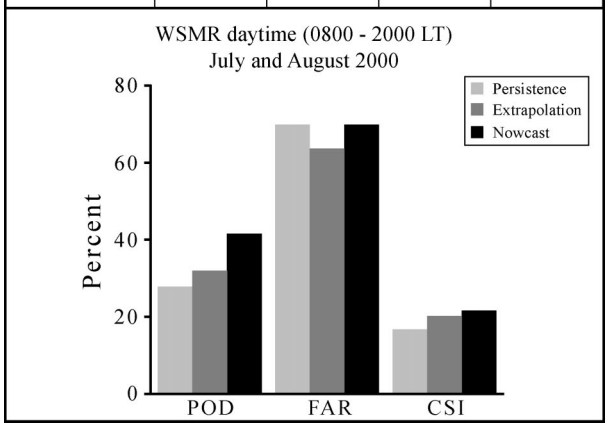

FIG. 15. Summary statistics from Jul and Aug 2000 for White Sands, NM, daytime 30-min nowcasts. The light gray, medium gray, and black bars represent the persistence, extrapolation, and ANC scores, respectively. The observations and nowcasts were expanded 3 km in all directions prior to the grid-to-grid comparisons.

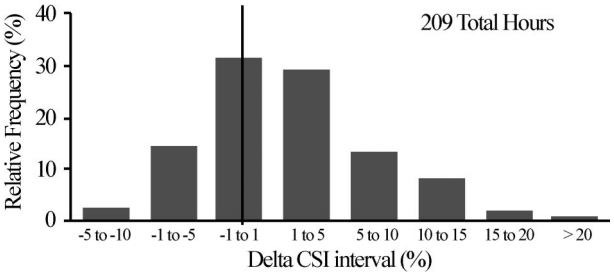

FIG. 16. Frequency distribution of the difference between ANC and extrapolation nowcasts calculated every 5 min. Positive values indicate the amount of improvement of ANC over extrapolation as measured by CSI.

marily dependent on radar and satellite observations of the current and developing storms and trends in their size. Although accurate 30-min nowcasts of storms are significantly affected by boundary detection, the determination of boundary characteristics is not so crucial for 30-min nowcasts as compared to the 60-min nowcasts. At longer time periods, current storms and trends are less important to the nowcasts because the life cycle of convective elements is generally less than an hour (Battan 1953; Foote and Mohr 1979; Henry 1993). Accurately nowcasting boundary layer forcing, shear, and instability becomes more important. Thus, boundary detection and extrapolation need to be accurate. With today's technology, consistently accurate boundary detections and extrapolations require a forecaster's input. The capability for real-time human input to help guide the automated system is currently incorporated into ANC. Additional effort is required to ensure the temporal continuity of the boundaries.

Correctly extrapolating the various predictor fields, which all tend to move with different motion vectors, is another difficult problem that tends to compound with longer nowcast intervals. Extrapolating the positions of objects that have a steady motion for at least three time periods is generally good. However in many cases motions are not steady or there is not a history. Important situations that are often incorrectly predicted include clouds not moving with the steering-level winds and instead remaining attached to the boundary, thus moving with the boundary motion; severe storms becoming right movers or developing a bow; boundaries stalling or accelerating; and initial storm motions being incorrectly based on steering-level winds when the storm is in fact tied to a forcing feature such as terrain or boundaries.

Stability issues also become more important as the nowcast period and domain increase. Currently, ANC

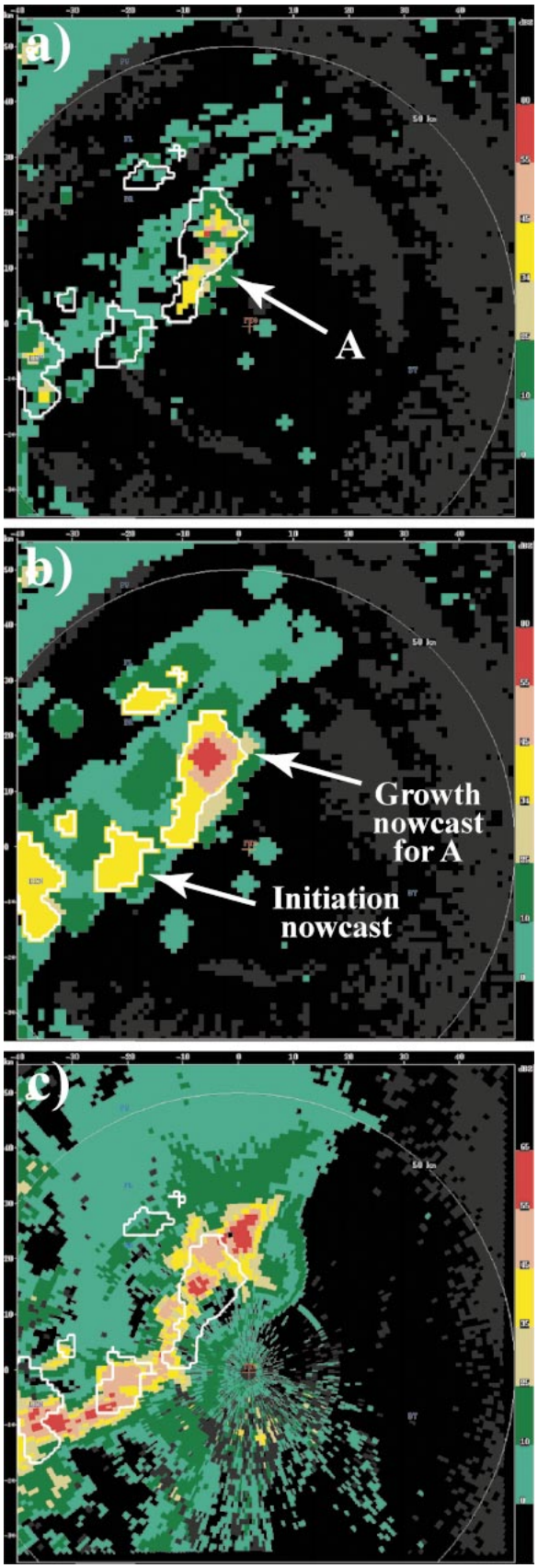

→

FIG. 17. Example of 60-min nowcast of reflectivity. Images show (a) the extrapolated reflectivity field, (b) the ANC reflectivity field nowcast, and (c) verification. The normal ANC nowcast is shown as a white contours in all three images. This nowcast was issued at 0000 UTC, which corresponds to Fig. 10b. Color scales as in Fig. 10.

uses clouds as a proxy for stability since there is no operationally direct means for obtaining high-resolution stability information. The use of clouds works well for short periods (0–30 min), but longer-period nowcasts require more direct measurements and nowcasts of stability. Efforts are on going to incorporate stability parameters from mesoscale numerical models into ANC. New water vapor observing technologies are also being closely followed. Presently the convergence and vertical motion associated with boundaries are based on retrievals from VDRAS. Efforts are under way to enhance VDRAS to forecast boundary layer winds for periods of 1–2 h.

A new algorithm in ANC nowcasts the reflectivity field and precipitation rate instead of the single nowcast contour shown in Figs. 8 and 10. An example of a 60-min reflectivity field nowcast is shown in Fig. 17. In this algorithm, two combined likelihood fields are generated: 1) likelihood for storm initiation and 2) likelihood for storm growth, maintenance, or dissipation. These fields are used to either initiate new storms (generally at an intensity of 35 dBZ) or to grow, maintain, or decrease the size of existing storms extrapolated to a new position. Figure 17a shows the existing echo in the extrapolated position. The resultant ANC reflectivity field is shown in Fig. 17b. The areas of growth and initiation are identified. The reflectivity field can be mapped to precipitation rate based on a Z–R relationship. Although promising results have been achieved using this method, much work is still required to accurately forecast intensity.

Acknowledgments. The authors would like to thank Brant Foote and Barbara Brown for their insightful comments on an earlier version of this paper. The FAA Aviation Weather Research Program, particularly Dave Pace, has provided continued support of the development of ANC through Interagency Agreement 98C00031. Collaboration with MIT/LL, particularly Marilyn Wolfson, Bob Hollowell, and Barb Forman, have been beneficial to the design and development of ANC. Dan Megenhardt is thanked for drafting the figures. Two anonymous reviewers made positive contributions to the paper. The Army Test and Evaluation Command has supported the installation and operation of ANC at the White Sands Missile Range and Redstone Arsenal. The U.S. Weather Research Program and the Nexrad Operational Support Facility supported the running of ANC during SCAN. Steven Zubrick, the NWS SOO, and forecaster John Margraf are thanked for their analysis and reconstruction of the 2 June synoptic and mesoscale events; Eric Hatfield is acknowledged for providing valuable forecast input on the ANC system running at White Sands.

REFERENCES

Bankert, R. L., 1994: Cloud classification of AVHRR imagery in maritime regions using a probablistic neural network. *J. Appl. Meteor.*, **33,** 909–918.

Battan, L. J., 1953: Duration of convective radar cloud units. *Bull. Amer. Meteor. Soc.*, **34,** 227–228.

Bernstein, B. C., F. McDonough, M. K. Politovich, and B. G. Brown, 2000: A research aircraft verification of the Integrated Icing Diagnostic Algorithm (IIDA). Preprints, *Ninth Conf. on Aviation, Range, and Aerospace Meteorology*, Orlando, FL, Amer. Meteor. Soc., 280–285.

Boldi, R. A., M. M. Wolfson, R. J. Johnson Jr., K. E. Theriault, B. E. Forman, and C. A. Wilson, 2002: An automated, operational two hour convective weather forecast for the corridor integrated weather. Preprints, *10th Conf. on Aviation, Range, and Aerospace Meteorology*, Portland, OR, Amer. Meteor. Soc., 116–119.

Byers, H. R., and R. R. Braham Jr., 1949: *The Thunderstorm.* U.S. Govt. Printing Office, 187 pp.

Cornman, L. B., R. K. Goodrich, C. S. Morse, and W. L. Ecklund, 1998: A fuzzy logic method for improved moment estimation from Doppler spectra. *J. Atmos. Oceanic Technol.*, **15,** 1287–1305.

Crook, N. A., 1996: Sensitivity of moist convection forced by boundary layer processes to low-level thermodynamic fields. *Mon. Wea. Rev.*, **124,** 1767–1785.

Delanoy, R. L., and S. W. Troxel, 1993: A machine intelligent gust front algorithim for Doppler weather radars. Preprints, *Fifth, Int. Conf. on Aviation Weather Systems*, Vienna, VA, Amer. Meteor. Soc., 125–129.

Dixon, M., and G. Wiener, 1993: TITAN: Thunderstorm Identification, tracking, Analysis and Nowcasting—A radar-based methodology. *J. Atmos. Oceanic Technol.*, **10,** 785–797.

Doswell, C. A., 1986: Short-range forecasting. *Mesoscale Meteorology and Forecasting*, P. Ray, Ed., Amer. Meteor. Soc., 689–707.

Foote, G. B., and C. G. Mohr, 1979: Results of a randomized hail suppression experiment in northeast Colorado. Part VI: Post hoc stratification by storm type and intensity. *J. Appl. Meteor.*, **18,** 1589–1600.

Golding, B. W., 1998: Nimrod: A system for generating automated very short range forecasts. *Meteor. Appl.*, **5,** 1–16.

Henry, S. G., 1993: Analysis of thunderstorm lifetime as a function of size and intensity. Preprints, *26th Conf. on Radar Meteorology*, Norman, OK, Amer. Meteor. Soc., 138–140.

——, and J. W. Wilson, 1993: Developing thunderstorm forecast rules utilizing first detectable cloud radar echoes. Preprints, *Fifth Conf. on Aviation Weather Systems*, Vienna, VA, Amer. Meteor. Soc., 304–307.

Johnson, J. T., P. L. MacKeen, A. Witt, E. D. Mitchell, G. J. Stumpf, M. D. Eilts, and K. W. Thomas, 1998: The storm cell identification and tracking algorithm: An enhanced WSR-88D algorithm. *Wea. Forecasting*, **13,** 263–276.

Keenan, T., and Coauthors, 2003: The Sydney 2000 World Weather Research Programme Forecast Demonstration Project: Overview and current status. *Bull. Amer. Meteor. Soc.*, in press.

Kessinger, C., S. Ellis, and J. Van Andel, 2001: NEXRAD data quality: The AP clutter mitigation scheme. Preprints, *30th Conf. on Radar Meteorology*, Munich, Germany, Amer. Meteor. Soc., 707–709.

Knight, C. A., and L. J. Miller, 1993: First radar echoes from cumulus clouds. *Bull. Amer. Meteor. Soc.*, **74,** 179–188.

Ligda, M. G., 1953: The horizontal motion of small precipitation areas as observed by radar. Tech. Rep. 21, Dept. of Meteorology, Massachusetts Institute of Technology, Cambridge, MA, 60 pp.

MacKeen, P. L., H. E. Brooks, and K. L. Elmore, 1999: Radar reflectivity–derived thunderstorm parameters applied to storm longevity forecasting. *Wea. Forecasting*, **14,** 289–295.

McNeill, D., and P. Freiberger, 1993: *Fuzzy Logic: The Revolutionary Computer Technology that is Changing Our World.* Simon and Schuster, 319 pp.

Megenhardt, D., C. K. Mueller, N. Rehak, and G. Cunning, 2000: Evaluation of the National Convective Weather Forecast Product. Preprints, *Ninth Conf. on Aviation, Range, and Aerospace Meteorology*, Orlando, FL, Amer. Meteor. Soc., 171–176.

Mueller, C. K., J. W. Wilson, and N. A. Crook, 1993: Utility of

soundings and mesonets to forecast thunderstorm initiation. *Wea. Forecasting,* **8,** 132–146.

——, F. McDonough, and J. W. Wilson, 1997: Forecasting the extent and lifetime of thunderstorm complexes for aviation applications. Preprints, *Seventh Conf. on Aviation, Range, and Aerospace Meteorology,* Long Beach, CA, Amer. Meteor. Soc., 244–248.

Pierce, C. E., and P. J. Hardaker, 2000: GANDOLF: A system for generating automated nowcasts of convective precipitation. *Meteor. Appl.,* **7,** 341–360.

Purdom, J. F. W., 1973: Satellite imagery and the mesoscale convective forecast problem. Preprints, *Eighth Conf. on Severe Local Storms,* Denver, CO, Amer. Meteor. Soc., 244–251.

——, 1976: Some uses of high resolution GOES imagery in the mesoscale forecasting of convection and its behavior. *Mon. Wea. Rev.,* **104,** 1474–1483.

——, 1982: Subjective interpretations of geostationary satellite data for nowcasting. *Nowcasting,* K. Browning, Ed., Academic Press, 149–166.

Rinehart, R. E., 1981: A pattern-recognition technique for use with conventional weather radar to determine internal storm motions. *Recent Progress in Radar Meteorology,* R. Carbone, Ed., Research Atmospheric Technology, Vol. 13, National Center for Atmospheric Research, 105–118.

Roberts, R. D., 1997: Detecting and forecasting cumulus cloud growth using radar and multi-spectral satellite data. Preprints, *28th Conf. on Radar Meteorology,* Austin, TX, Amer. Meteor. Soc., 408–409.

——, and S. Rutledge, 2003: Nowcasting storm initiation and growth using *GOES-8* and WSR-88D data. *Wea. Forecasting,* **18,** 562–584.

——, T. Saxen, C. Mueller, J. Wilson, A. Crook, J. Sun, and S. Henry, 1999: Operational application and use of NCAR's thunderstorm nowcasting system. Preprints, *15th Int. Conf. on Interactive Information and Processing Systems,* Dallas, TX, Amer. Meteor. Soc., 158–161.

Rotunno, R., J. B. Klemp, and M. L. Weisman, 1988: A theory for strong, long-lived squall lines. *J. Atmos. Sci.,* **45,** 463–485.

Saxen, T. R., C. K. Mueller, T. C. Jameson, and E. Hatfield, 1999: Determining key parameters for forecasting thunderstorms at White Sands Missile Range. Preprints, *Int. Conf. on Radar Meteorology,* Montreal, QC, Canada, Amer. Meteor. Soc., 9–12.

Sharman, R., B. G. Brown, and S. Dettling, 2000: Preliminary results of the NCAR Integrated Turbulence Forecasting Algorithm (ITFA) to forecast CAT. Preprints, *Ninth Conf. on Aviation, Range, and Aerospace Meteorology,* Orlando, FL, Amer. Meteor. Soc., 460–465.

Smith, S. B., J. T. Johnson, R. D. Roberts, S. M. Zubrick, and S. J. Weiss, 1998: The System for Convective Analysis and Nowcasting (SCAN): 1997–1998 field test. Preprints, *19th Conf. on Severe Local Storms,* Minneapolis, MN, Amer. Meteor. Soc., 790–793.

Steiner, M., R. A. Houze Jr., and S. E. Yuter, 1995: Climatological characterization of three-dimensional storm structure from operational radar and rain gauge data. *J. Appl. Meteor.,* **34,** 1978–2007.

Sun, J., and N. A. Crook, 2001: Real-time low-level wind and temperature analysis using single WSR-88D data. *Wea. Forecasting,* **16,** 117–132.

Tsonis, A. A., and G. L. Austin, 1981: An evaluation of extrapolation techniques for the short-term prediction of rain amounts. *Atmos.–Ocean,* **19,** 54–65.

Tuttle, J. D., and G. B. Foote, 1990: Determination of the boundary layer airflow from a single Doppler radar. *J. Atmos. Oceanic Technol.,* **7,** 218–232.

Vivekanandan, J., D. S. Zrnic, S. M. Ellis, R. Oye, A. V. Ryzhkov, and J. Straka, 1999: Cloud microphysics retrieval using S-band dual-polarization radar measurements. *Bull. Amer. Meteor. Soc.,* **80,** 381–388.

Weckwerth, T. M., 2000: The effect of small-scale moisture variability on thunderstorm initiation. *Mon. Wea. Rev.,* **128,** 4017–4030.

Wilks, D. S., 1995: *Statistical Methods in the Atmospheric Sciences: An Introduction.* Academic Press, 464 pp.

Wilson, J. W., 1966: Movement and predictability of radar echoes. Tech. Memo. ERTM-NSSL-28, National Severe Storms Laboratory, 30 pp.

——, and R. Carbone, 1984: Nowcasting with Doppler radar: The forecaster–computer relationship. *Nowcasting II,* K. Browning, Ed., European Space Agency, 177–186.

——, and W. E. Schreiber, 1986: Initiation of convective storms by radar-observed boundary layer convergent lines. *Mon. Wea. Rev.,* **114,** 2516–2536.

——, and C. K. Mueller, 1993: Nowcasts of thunderstorm initiation and evolution. *Wea. Forecasting,* **8,** 113–131.

——, and D. L. Megenhardt, 1997: Thunderstorm initiation, organization, and lifetime associated with Florida boundary layer convergence lines. *Mon. Wea. Rev.,* **125,** 1507–1525.

——, N. A. Crook, C. K. Mueller, J. Sun, and M. Dixon, 1998: Nowcasting thunderstorms: A status report. *Bull. Amer. Meteor. Soc.,* **79,** 2079–2099.

Wolfson, M. M., C. K. Mueller, and M. Eilts, 1997: Convective weather forecasting for FAA applications by the Convective Weather Product Development Team. Preprints, *Seventh Conf. on Aviation, Range, and Aerospace Meteorology,* Long Beach, CA, Amer. Meteor. Soc., 238–243.

——, G. E. Forman, R. G. Hallowell, and M. P. Moore, 1998: The growth and decay tracker. Preprints, *Eighth Conf. on Aviation, Range, and Aerospace Meteorology,* Dallas, TX, Amer. Meteor. Soc., 58–62.